

THE DEEP MINIMIZING MOVEMENT SCHEME*

HYUNG JU HWANG^{†§¶}, CHEOLHYEONG KIM[†], MIN SUE PARK[†], AND HWIJAE SON[‡]

Abstract. Solutions of certain partial differential equations (PDEs) are often represented by the steepest descent curves of corresponding functionals. Minimizing movement scheme was developed in order to study such curves in metric spaces. Especially, Jordan-Kinderlehrer-Otto studied the Fokker-Planck equation in this way with respect to the Wasserstein metric space. In this paper, we propose a deep learning-based minimizing movement scheme for approximating the solutions of PDEs. The proposed method is highly scalable for high-dimensional problems as it is free of mesh generation. We demonstrate through various kinds of numerical examples that the proposed method accurately approximates the solutions of PDEs by finding the steepest descent direction of a functional even in high dimensions.

Key words. Minimizing Movement Scheme, JKO Scheme, Neural Networks

AMS subject classifications. 68T07

1. Introduction. Starting from the pioneering concerns given in [12], the theory of gradient flow evolution in general metric spaces has been intensively studied to unify many problems in calculus of variations, differential equations, mean curvature flow, etc. In this trend, *minimizing movement scheme* [11] was devised as a general method for the study of steepest descent curves of a functional F in a metric space (X, d_X) , and this method was extensively applied to various differential equations as a time-implicit semi-discrete scheme.

Historically, the application of minimizing movement scheme to differential equations was exclusively based on gradient flows arising from a separable Hilbert space, particularly $L^2(\mathbb{R}^n)$. Later, in [18], Jordan, Kinderlehrer, and Otto observed that the Fokker-Planck equation can be understood as a steepest descent for the free energy with respect to the Wasserstein distance and utilized the minimizing movement scheme for Wasserstein spaces, and that is why the minimizing movement scheme is now widely known as the JKO-scheme (Jordan, Kinderlehrer and Otto). In recent years, it has been known that a large class of diffusion equations can be variationally reformulated as gradient flows in L^2 -Wasserstein spaces, and the minimizing movement scheme has now become a popular tool for deriving numerical schemes for these equations.

Neural networks have been considered as candidates for approximators of the solutions of PDEs in past decades. The earliest work dates back to the 1990s, for example, [21, 13]. However, due to the limitation of computing resources and the absence of an efficient training algorithm, the proposed neural network solvers were often undervalued at that time. Along with the recent advances in deep learning theory such as the back-propagation and the stochastic gradient descent algorithm, several approaches for solving PDEs via neural networks have been revisited. One major line of

*Submitted to the editors 07/09/21.

Funding: Funding information

[†]Department of Mathematics, Pohang University of Science and Technology, Pohang 790-784, Republic of Korea (minsuepark@postech.ac.kr, tyty4@postech.ac.kr, hjhwang@postech.ac.kr).

[‡]Stochastic Analysis and Application Research Center, Korea Advanced Institute of Science and Technology, Daejeon, Republic of Korea (son9409@kaist.ac.kr).

[§]Graduate School of Artificial Intelligence, Pohang University of Science and Technology, Pohang 790-784, Republic of Korea (hjhwang@postech.ac.kr).

[¶]Corresponding Author

research is Physics Informed Neural Networks (PINNs) [39], which proposed to train a neural network to minimize the sum of PDE residual functions. Plenty of works are then reported regarding the convergence property of continuous loss formulation [17, 16, 22], dealing with the exact imposition of the boundary condition [4, 35], works on improving training efficiency [42, 46, 30, 44], and applications to high-dimensional problems [41] to name a few. Another approach, called the deep Ritz method, reformulates a PDE problem into an optimization problem of a variational functional [47], and a corresponding convergence result is reported in [34]. Neural network solutions of variational problems with essential boundary conditions are studied in [25], and a pre-training strategy for the deep Ritz method condition is proposed in [9].

Traditional numerical schemes such as Finite Difference Method (FDM), Finite Element Method (FEM), Finite Volume Method (FVM) require fine mesh generation for an accurate approximation. Since mesh generation and computation become intractable as the computational dimension increases, they often fail to solve PDEs in high dimensions [27]. On the other hand, the aforementioned neural network methods have successful approximations in high-dimensional settings. For example, [41] proposed an iterative sampling technique together with the stochastic gradient descent to tackle the high-dimensional PDEs, and [41, 42] showed that neural networks could accurately approximate the solution in high dimensions. Additionally, [47] considers variational problems in high dimensions for elliptic PDEs. In this paper, we consider several high-dimensional PDEs as example problems to demonstrate the empirical success of our method.

Optimizing a functional and finding a minimizer have been widely studied both in the machine learning community and in the PDE literature. Recently, optimization of a functional defined on a space of probability measures equipped with L^2 -Wasserstein distance arises as an important problem. Therefore, Wasserstein gradient flow plays an important role in studying the steepest descent of a target functional in the space of probability measures. [1] and [32] proposed to applying JKO scheme with neural networks with tractable algorithms. However, their usage of JKO scheme mainly focused on a fast approximation of the steepest descent of the target functional, not on the accurate prediction of a whole dynamic system. For example, the experiment results of [1] on the Wasserstein gradient flow type PDEs were mainly discussed on its *asymptotic convergence of the objective functions*, but the accurate prediction of the solution $u(t, x)$ was not mentioned. Meanwhile, [26] proposed to solve Fokker-Planck equation with neural networks by emerging JKO scheme, Wasserstein Gradient Flow, and its geometric interpretation. However, its usage is limited to Fokker-Planck equation, since [26] projected the Fokker-Planck equation onto a parametric manifold with a new metric tensor and viewed the equation as a new ODE system on the manifold.

In this paper, we propose a neural network model which reflects the minimizing movement scheme for solving PDEs. Our proposed method has several advantages in the following aspects. Firstly, our method is more suitable for solving high-dimensional problems than the traditional mesh-based schemes [26] because the mesh generation is not necessary for the proposed method, and neural networks are capable of handling high-dimensional objects in general. Secondly, while specifying boundary condition often causes a problem in both residual minimization [35] and the deep Ritz method [9], it often follows naturally from the minimizing movement scheme in our method. Therefore, we do not need to explicitly specify boundary conditions for those PDEs derivable from the minimizing movement scheme. Lastly, our model easily enables time extrapolation of the numerical solution in contrast to residual minimization;

we only need to solve one more optimization problem for one-step time extrapolation, while the residual minimization requires additional training in the whole time-space domain. Furthermore, an increment of the error at each time step is bounded by $\mathcal{O}(\tau^{1/2})$, where τ denotes the step size. See, theorem 3.1.

2. Preliminaries.

2.1. Gradient flow. In general, given a Riemannian manifold (M, g) , a curve $u : (0, \infty) \rightarrow M$ is said to be the *gradient flow* of a smooth functional $\mathcal{F} : M \rightarrow \mathbb{R}$ if it follows the direction in which \mathcal{F} decreases at most. Formally, this definition can be interpreted by the evolution equation

$$(2.1) \quad \frac{d}{dt}u(t) = -\nabla_M \mathcal{F}(u(t)).$$

If M is a Hilbert space, the gradient of \mathcal{F} is given by its functional derivative, which is derived from the Riesz representation of the Fréchet derivative $D\mathcal{F}$ of \mathcal{F} : $D\mathcal{F}(x)(y) = \langle \nabla_X \mathcal{F}(x), y \rangle$ for every $x, y \in M$. Therefore, for $\Omega \subset \mathbb{R}^n$, $\nabla_{L^2(\Omega)} \mathcal{F}(u)$ is merely the functional derivative $\frac{\delta \mathcal{F}}{\delta u}(u)$ since $L^2(\Omega)$ is itself a Hilbert space.

For example, the heat equation $\frac{d}{dt}u(t) = \Delta u$ is the gradient flow of the Dirichlet energy $\mathcal{F}(u) := \frac{1}{2} \int \|\nabla u\|^2 dx$ in $L^2(\mathbb{R}^n)$ because $\nabla_{L^2(\mathbb{R}^n)} \mathcal{F}(u) = \frac{\delta \mathcal{F}}{\delta u}(u) = -\Delta u$.

As illustrated in the above example, to reformulate an evolution equation into its variational form as in (2.1), finding an appropriate Riemannian manifold (M, g) would be helpful. An important and interesting example of such Riemannian manifold was observed in [37] that there is a metric tensor g which induces the L^2 -Wasserstein metric \mathbb{W}_2 on $\mathcal{P}_2(\Omega)$, the space of Borel probability distributions on $\Omega \subset \mathbb{R}^n$ with finite second moments. Here, Ω is assumed to be either an open bounded subset of \mathbb{R}^n with smooth boundary or \mathbb{R}^n . Abusing notation and identifying the absolutely continuous measure u with its density as $du(x) = u(x)dx$, it was shown in [37] that, under some assumptions on \mathcal{E} , the gradient $\nabla_{\mathbb{W}_2} \mathcal{E}(u)$ can be explicitly expressed by

$$(2.2) \quad \nabla_{\mathbb{W}_2} \mathcal{F}(u) = -\nabla \cdot (u \nabla \frac{\delta \mathcal{F}}{\delta u}(u)).$$

In general, many interesting linear functionals \mathcal{F} on $(\mathcal{P}_2(\mathbb{R}^n), \mathbb{W}_2)$ are given as linear combinations of three types of basic functionals; potential energy $\mathcal{V}(u) := \int V u$, interaction energy $\mathcal{W}(u) := \int (W * u)u$, and internal energy $\mathcal{E}(u) := \int u \phi(u)$ where these energies are defined for absolutely continuous u 's and defined by ∞ otherwise. For example, the heat equation $\frac{d}{dt}u(t) = \nabla u$ is also the gradient flow of the entropy $\mathcal{E} : (\mathcal{P}_2(\mathbb{R}^n), \mathbb{W}_2) \rightarrow [0, +\infty]$ defined by $\int u(x) \log u(x) dx$ for absolutely continuous u and ∞ otherwise, because $\nabla \cdot (u \nabla \frac{\delta \mathcal{E}}{\delta u}(u)) = \Delta u$.

Examples of basic functionals and their corresponding gradient flows on $L^2(\mathbb{R}^n)$ and $(\mathcal{P}_2(\Omega), \mathbb{W}_2)$ are given in Table 2.1.

2.2. Minimizing movement scheme (JKO scheme). A metric space (X, d_X) is said to be a geodesic space if $d_X(x, y)$ is a geodesic between x and $y \in X$ for every x and $y \in X$. It is well-known that if a metric space X is a geodesic Polish space, then $(\mathcal{P}_2(X), \mathbb{W}_2)$ is a geodesic Polish space as well, and any Hilbert space is a geodesic space [2]. Therefore, for any convex subset $\Omega \subset \mathbb{R}^n$, $L^2(\Omega)$ and $(\mathcal{P}_2(\Omega), \mathbb{W}_2)$ are geodesic Polish spaces.

Let (X, d_X) be a geodesic Polish space with Riemannian structure and $F : X \rightarrow \mathbb{R} \cup \{+\infty\}$ be a lower semi-continuous λ -geodesically convex function (under suitable

	Functional	Gradient Flow
$L^2(\mathbb{R}^n)$	$\mathcal{F}(u) = \int \phi(u)$	$\frac{d}{dt}u(t) = -\phi'(u)$
	$\mathcal{F}(u) = \int \ \nabla u\ ^2$	$\frac{d}{dt}u(t) = \Delta u$
	$\mathcal{F}(u) = \int u(x)f(x)$	$\frac{d}{dt}u(t) = -f(x)$
\mathbb{W}_2	$\mathcal{F}(u) = \int u \log u$	$\frac{d}{dt}u(t) = \Delta u$
	$\mathcal{F}(u) = \frac{1}{m-1} \int u^m$	$\frac{d}{dt}u(t) = \Delta u^m$
	$\mathcal{F}(u) = \int V u$	$\frac{d}{dt}u(t) = \nabla \cdot (\nabla V u)$
	$\mathcal{F}(u) = \int (W * u)u$	$\frac{d}{dt}u(t) = \nabla \cdot (\nabla (W * u)u)$

Table 2.1: Examples of functionals and their corresponding gradient flows.

compactness assumptions to guarantee existence of the minimum), and iteratively define

$$(2.3) \quad x_{k+1}^\tau = \arg \min_{x \in X} \left\{ \mathcal{F}(x) + \frac{d_X(x, x_k^\tau)^2}{2\tau} \right\}, \quad x_0^\tau = x_0,$$

for $\tau > 0$ and some initial point $x_0 \in X$ such that $E(x_0) < +\infty$.

This scheme is said to be the *minimizing movement scheme*. If we define a curve such that $x^\tau(k\tau) = x_k^\tau$ and such that x^τ restricted on any interval $[k\tau, (k+1)\tau]$ is a constant-speed geodesic with speed $\frac{d(x_k^\tau, x_{k+1}^\tau)}{\tau}$, up to a subsequence $\tau_j \rightarrow 0$, x^τ converges uniformly to the solution of (2.1) if some regularity conditions on \mathcal{F} and (X, d_X) are assumed.

Moreover, a gradient flow derived through the minimizing movement scheme in $L^2(\Omega)$ is always accompanied by the boundary condition $\frac{\delta \phi}{\delta(\nabla u)} \cdot \hat{\mathbf{n}}$ on $\partial\Omega$ when the functional \mathcal{F} is given in the form $\mathcal{F}(u) := \int \phi(u, \nabla u)$, if Ω is not \mathbb{R}^n itself [5]. Likewise, a gradient flow derived through the minimizing movement scheme in $(\mathcal{P}_2(\Omega), \mathbb{W}_2)$ is always accompanied by no-flux boundary condition on $\partial\Omega$, i.e. $u \nabla \frac{\delta \mathcal{F}}{\delta u}(u) \cdot \hat{\mathbf{n}} = 0$, if Ω is not \mathbb{R}^n itself [40].

In particular, the gradient flows of the heat equation and the Allen-Cahn equation derived through the minimizing movement scheme in the space $L^2(\Omega)$ satisfy the Neumann boundary condition [5, 31]. Similarly, the gradient flow of the heat equation derived through the minimizing movement scheme in the space $(\mathcal{P}_2(\Omega), \mathbb{W}_2)$ satisfies the Neumann boundary condition [2]. In this paper, we consider Neumann boundary conditions when $\Omega \neq \mathbb{R}^n$.

2.3. Optimal transport and L^2 -Wasserstein distance. Let μ, ν be Borel probability measures on Polish spaces X, Y respectively. Given a cost function $c : X \times Y \rightarrow [0, +\infty]$ where $c(x, y)$ measures the cost of transporting one unit of mass from $x \in X$ to $y \in Y$, the *optimal transport problem* is how to transport μ to ν while minimizing the cost c . This was firstly formulated by Monge [33] as follows:

$$(2.4) \quad (MP) \quad \inf_{T_*\mu = \nu} \int_X c(x, T(x)) d\mu(x),$$

where $T : X \rightarrow Y$ are measurable maps (transport maps).

However, this problem is ill-posed because of the constraint $T_*\mu = \nu$. For instance, if μ is a Dirac measure and ν is not, there is no admissible T . Later, Kantorovich

proposed the following way to relax the Monge problem:

$$(2.5) \quad (KP) \quad \min_{\gamma \in \Pi(\mu, \nu)} \int_{X \times Y} c(x, y) d\gamma(x, y),$$

where $\Pi(\mu, \nu)$ is the collection of joint distributions (transport plans) of μ and ν .

Moreover, if μ is non-atomic and c is continuous, then there always exist optimal transport plans satisfying (2.5) and it coincides with the infimum of (2.4) [38]. In particular, this is the case when $X = Y = \mathbb{R}^n$ and $c(x, y) := \|x - y\|_2^2$. The L^2 -Wasserstein distance between μ and ν is defined to be the square root of the minimum of (2.5) when $c(x, y) := \|x - y\|_2^2$, and is denoted by $\mathbb{W}_2(\mu, \nu)$.

Estimation of L^2 -Wasserstein distance is essential for solving PDEs with JKO scheme and applying optimal transport in a machine learning area. Previous studies [43, 28] proposed to estimate this L^2 -Wasserstein distance by applying Kantorovich-Rubinstein duality theorem [45] and approximating primal/conjugate convex functions. However, their computations were based on minimax optimization, which leads to a heavy computational cost and a slow estimation speed.

Meanwhile, the authors in [20] proposed Wasserstein-2 generative networks (W2GN), an end-to-end non-minimax algorithm for training optimal transport mappings for L^2 -Wasserstein distance. They avoided the minimax optimization by introducing a regularization term on the convex conjugate potential. Instead of optimizing minimax problem, W2GN simply minimizes the cost and controls the conjugate function. Compared with the previous minimax-based computation algorithms in [43, 28], W2GN significantly improves the computational cost for estimating L^2 -Wasserstein distance.

In the rest of this subsection, we briefly describe the method for estimating $\mathbb{W}_2(\mu, \nu)$, that was proposed in [20].

When absolutely continuous distributions u, ρ with finite second moments are given, by re-arranging the Monge's formulation (2.4), $\mathbb{W}_2(u, \rho)$ can be expressed by

$$(2.6) \quad \mathbb{W}_2^2(u, \rho) = \int_{\mathbb{R}^n} \|x\|^2 du(x) + \int_{\mathbb{R}^n} \|y\|^2 d\rho(y) - 2 \cdot \max_{T_* u = \rho} \int_{\mathbb{R}^n} \langle x, T(x) \rangle du(x).$$

We denote the maximum term on the right hand side of (2.6) by $\text{Corr}(u, \rho)$, and $-\text{Corr}(u, \rho)$ can be regarded as (2.4) for $c(x, y) := -\langle x, y \rangle$ [29]. Therefore, by applying the Kantorovich-Rubinstein duality theorem, we have

$$(2.7) \quad \text{Corr}(u, \rho) = \min_{\psi \in \text{Convex}} \left[\int_{\mathbb{R}^n} \psi(x) du(x) + \int_{\mathbb{R}^n} \bar{\psi}(y) d\rho(y) \right],$$

where the minimum is taken over all the convex functions $\psi : \mathbb{R}^n \rightarrow \mathbb{R} \cup \{+\infty\}$, and $\bar{\psi}(y) := \max_{x \in \mathbb{R}^n} (\langle x, y \rangle - \psi(x))$ is the Fenchel convex conjugate to ψ .

According to [45, 29], the gradient $T^* := \nabla \psi^*$ of the optimal ψ^* readily gives the maximizer of (2.6), and we have

$$(2.8) \quad (T^*)^{-1}(y) = (\nabla \psi^*)^{-1}(y) = \nabla \bar{\psi}^*(y).$$

Therefore, it suffices to find the minimizer ψ of (2.7) to evaluate the L^2 -Wasserstein distance $\mathbb{W}_2(u, \rho)$. However, to do this, we need to solve the optimization sub-problem

$\bar{\psi}(y) = \max_{x \in \mathbb{R}^n} (\langle x, y \rangle - \psi(x))$, and this would lead to a minimax problem

$$\begin{aligned}
& \min_{\psi \in \text{Convex}} \left[\int_{\mathbb{R}^n} \psi_{\theta}(x) du(x) + \int_{\mathbb{R}^n} \bar{\psi}(y) d\rho(y) \right] \\
&= \min_{\psi \in \text{Convex}} \left[\int_{\mathbb{R}^n} \psi_{\theta}(x) du(x) + \int_{\mathbb{R}^n} [\max_{x \in \mathbb{R}^n} \langle x, y \rangle - \psi(x)] d\rho(y) \right] \\
(2.9) \quad &= \min_{\psi \in \text{Convex}} \left[\int_{\mathbb{R}^n} \psi_{\theta}(x) du(x) + \max_{S: \mathbb{R}^n \rightarrow \mathbb{R}^n} \int_{\mathbb{R}^n} [\langle S(y), y \rangle - \psi(S(y))] d\rho(y) \right]
\end{aligned}$$

where the maximum is taken over arbitrary measurable functions S .

Nevertheless, [20] proposed a trick to convert this problem into an end-to-end non-minimax problem by considering the optimal ψ and $\bar{\psi}$. For the variational approximation in (2.9), we obtain a variational lower bound which matches the entire value for $S = (\nabla \psi)^{-1}(y) = \nabla \bar{\psi}(y)$.

Therefore, the primal potential ψ and its conjugate $\bar{\psi}$ can be approximated by two parametrized convex functions ψ_{θ} and $\bar{\psi}_{\omega}$ respectively, if we minimize the following objective:

$$(2.10) \quad \min_{\theta, \omega} \left[\int_{\mathbb{R}^n} \psi_{\theta}(x) du(x) + \int_{\mathbb{R}^n} [\langle \nabla \bar{\psi}_{\omega}(y), y \rangle - \psi_{\theta}(\nabla \bar{\psi}_{\omega}(y))] d\rho(y) \right].$$

Moreover, the relation (2.8) must be imposed to the optimized pair $(\psi_{\theta}, \bar{\psi}_{\omega})$, and this can be done by additionally minimizing the following regularization:

$$(2.11) \quad R(\theta, \omega) := \int_{\mathbb{R}^n} \|\nabla \psi_{\theta} \circ \nabla \bar{\psi}_{\omega}(y) - y\|^2 d\rho(y).$$

In conclusion, our final objective would be the following:

$$(2.12) \quad \min_{\theta, \omega} \left[\int_{\mathbb{R}^n} \psi_{\theta}(x) du(x) + \int_{\mathbb{R}^n} [\langle \nabla \bar{\psi}_{\omega}(y), y \rangle - \psi_{\theta}(\nabla \bar{\psi}_{\omega}(y))] d\rho(y) + \lambda \cdot R(\theta, \omega) \right],$$

where $\lambda > 0$ is a hyperparameter.

Using the identities (2.6) and (2.7), once the optimal $\psi_{\theta^*}, \bar{\psi}_{\omega^*}$ are found, $\mathbb{W}_2(u, \rho)$ can now be approximated by the following:

$$(2.13) \quad \int_{\mathbb{R}^n} \|x\|^2 du(x) + \int_{\mathbb{R}^n} \|y\|^2 d\rho(y) - 2 \cdot \left[\int_{\mathbb{R}^n} \psi_{\theta^*}(x) du(x) + \int_{\mathbb{R}^n} \bar{\psi}_{\omega^*}(y) d\rho(y) \right]$$

The remaining obstacle is to find the optimal ψ_{θ^*} and $\bar{\psi}_{\omega^*}$ with a tractable computation. In order to find them and to use them as approximated solutions of ψ^* and $\bar{\psi}^*$, a large enough but tractable space of parametrized convex functions should be introduced. Here, we used input convex neural network (ICNN) architectures to approximate the optimal convex functions, which were firstly presented in [3]. Recently, ICNN architectures are widely chosen to approximate the optimal convex potential and its conjugate in the previous studies [43, 28, 20, 1, 32]. Among them, a fully-convex, k -layer, fully-connected ICNN (FICNN) architecture was proposed

$$z_{i+1} = g_i(W_i^{(z)} z_i + W_i^{(y)} y + b_i), \quad 0 \leq i \leq k-1, \quad W_0^{(z)} = 0$$

where y denotes an input, g_i denotes the activation function, and z_k denotes the final output. Let $\theta := \{W_{0:k-1}^{(y)}, W_{1:k-1}^{(z)}, b_{0:k-1}\}$ be the parameters of k -layer FICNN $f(y; \theta) = z_k$. The authors in [3] claimed that the function f is convex with respect to y given $W_{1:k-1}^{(z)}$ are non-negative and g_i are non-decreasing convex activation functions.

2.4. Universal approximation theorem. The approximation theory of the neural network has been widely studied in past decades after a seminal work [10] which states the universal approximation property of one hidden layer neural network with sigmoidal activations.

The original result had been generalized in many directions. For example, [15] showed the approximation property for more general activation functions.

THEOREM 2.1 (Theorem 2 in [15]). *Whenever σ is continuous, bounded and non-constant, the the finite sums of the form*

$$(2.14) \quad G(x) = \sum_{j=1}^N a_j \sigma(y_j^T x + \theta_j)$$

is dense in $C(X)$ for all compact sets $X \subset \mathbb{R}^n$.

Later, the authors in [23] showed that being a universal approximator is equivalent to have a non-polynomial activation function σ . Approximation theorems in space of differentiable functions are established in [24] through the following theorem.

THEOREM 2.2 (Theorem 2.1 in [24]). *Let X be a compact subset of \mathbb{R}^n . and $f \in \hat{C}^{m_1}(X) \cap \hat{C}^{m_2}(X) \cap \dots \cap \hat{C}^{m_q}(X)$, where $m_i \in \mathbb{Z}_+^n$. Also, let σ be any non-polynomial function in $C^n(\mathbb{R})$, where $n = \max\{|m_i|, 1 \leq i \leq q\}$. Then for any $\epsilon > 0$, there is a neural network defined as in (2.14) such that*

$$\|D^k f - D^k G\|_{L^\infty(X)} < \epsilon, \quad k \leq m_i, \quad \text{for some } i, 1 \leq i \leq q.$$

The density argument on simultaneous approximations of multivariate functions and their partial derivatives have been applied to show the existence of a neural network that arbitrarily minimizes the PDE residual loss function, see [17, 41].

3. The Deep Minimizing Movement Method. We consider the following sequential minimization problem with time step τ :

$$(3.1) \quad u_{k+1} = \arg \min_{u \in X} \left\{ \mathcal{F}(u) + \frac{d_X^2(u, u_k)}{2\tau} \right\}, \quad u_0 = u(0, x),$$

where X denotes either $L^2(\Omega)$, or $\mathcal{P}_2(\Omega)$ with L^2 -Wasserstein distance.

The main idea of this paper is to optimize (3.1) by parametrizing u by neural network u_θ . We begin this section by showing that the increment of the error at each update is bounded above.

THEOREM 3.1. *Let X be a metric space and $\mathcal{F} : X \rightarrow \mathbb{R} \cup \{+\infty\}$ be a lower semi-continuous function with some lower bounds to guarantee the existence of minimizers of (3.1) for small τ . Given $u_0 \in X$ with $\mathcal{F}(u_0) < \infty$, let $\{u_k\}$ be the true minimizers of (3.1) for each k , and let $\{u_{\theta,k}\}$ be a sequence of neural network approximation obtained by solving the optimization problem (3.1) iteratively with a natural assumption that $\mathcal{F}(u_{\theta,k+1}) + \frac{d_X^2(u_{\theta,k+1}, u_{\theta,k})}{2\tau} \leq \mathcal{F}(u_{\theta,k}) + \frac{d_X^2(u_{\theta,k}, u_{\theta,k})}{2\tau}$ for each k . Then, we obtain*

$$d_X(u_{\theta,k+1}, u_{k+1}) \leq d_X(u_{\theta,k}, u_k) + C\tau^{1/2}$$

for some constant C depending on \mathcal{F} and initial u_0 .

Proof. Firstly, since u_{k+1} is the minimizer of (3.1), we get

$$\mathcal{F}(u_{k+1}) + \frac{d_X^2(u_{k+1}, u_k)}{2\tau} \leq \mathcal{F}(u_k) + \frac{d_X^2(u_k, u_k)}{2\tau} = \mathcal{F}(u_k)$$

Therefore, we get $\mathcal{F}(u_{k+1}) \leq \mathcal{F}(u_k)$ for each k . Since this is valid for every k , we have $\mathcal{F}(u_k) \leq \mathcal{F}(u_0) < +\infty$ for each k . Analogous arguments applies to $u_{\theta,k}$, and we conclude that $\mathcal{F}(u_{\theta,k}) < +\infty$ for each k .

Again, by the definition of u_k 's, we get

$$d_X^2(u_k, u_{k+1}) \leq 2\tau(\mathcal{F}(u_k) - \mathcal{F}(u_{k+1})) \leq 2\tau(\mathcal{F}(u_0) - \inf \mathcal{F}) = 2A\tau$$

where $A = A(u_0, \mathcal{F}) := (\mathcal{F}(u_0) - \inf \mathcal{F})$ only depends on the functional \mathcal{F} and the initial u_0 . Analogously, by the assumption, we get $d_X^2(u_{\theta,k}, u_{\theta,k+1}) < 2A\tau$. Then,

$$\begin{aligned} d_X(u_{\theta,k+1}, u_{k+1}) &\leq d_X(u_{\theta,k+1}, u_{\theta,k}) + d_X(u_{\theta,k}, u_k) + d_X(u_k, u_{k+1}) \\ &< \sqrt{2A\tau} + d_X(u_{\theta,k}, u_k) + \sqrt{2A\tau} = d_X(u_{\theta,k}, u_k) + C\tau^{1/2} \end{aligned}$$

where $C = 2\sqrt{2A}$. □

In the remaining of this section, we give a detailed description of the framework of our method for the spaces $L^2(\Omega)$ and $\mathcal{P}_2(\Omega)$ with L^2 -Wasserstein distance.

3.1. Case when $X = L^2(\Omega)$. If $X = L^2(\Omega)$ and the functional $\mathcal{F}(u)$ is given in the form $\int \phi(u, \nabla u)$, this integration can be evaluated by Monte Carlo estimate over mini-batches from the uniform distribution on Ω if Ω is bounded. If $\Omega = \mathbb{R}^n$, we can still approximate this integration by restricting the domain to a sufficiently large cropped bounded subset, i.e. $\int_{\mathbb{R}^n} \phi(u, \nabla u) \approx \int_{[-M, M]^n} \phi(u, \nabla u)$. Likewise, the distance $d_{L^2(\Omega)}^2(u, v) = \int_{\Omega} \|u - v\|^2$ can also be evaluated by Monte Carlo estimate in the same manner. Since $C_c^\infty(\Omega)$ is dense in $L^2(\Omega)$ and any function $f \in C_c^\infty(\Omega)$ can be approximated by a neural network u_θ according to Theorem 2.2, it suffices to minimize

$$(3.2) \quad \arg \min_{\theta} \left\{ \int \phi(u_\theta, \nabla u_\theta) + \frac{d_{L^2(\Omega)}^2(u_\theta, u_k)}{2\tau} \right\},$$

for a given u_k to obtain the minimizer $u_{\theta^*(k+1)}$, which is an approximation of the minimizer of (3.1). Then, we take the optimized $u_{\theta^*(k+1)}$ in place of u_k and repeat this process iteratively to derive the corresponding time-discretized gradient flow.

3.2. Case when $X = \mathcal{P}_2(\Omega)$. If $X = \mathcal{P}_2(\Omega)$ and the functional $\mathcal{F}(u)$ is given as a linear combination of potential energy \mathcal{V} and interaction energy \mathcal{W} and internal energy \mathcal{E} , there is no problem approximating $\mathcal{F}(u)$ by Monte Carlo estimate as described in Section 3.1. Moreover, since $C_c^\infty(\Omega)$ is dense in $L^1(\Omega)$ and any function $f \in C_c^\infty(\Omega)$ can be approximated by a neural network by Theorem 2.2, any probability density function can be approximated by a neural network u_θ having non-negative outputs. Therefore, if we define $\widetilde{u}_\theta := \frac{1}{\int u_\theta} u_\theta$ for non-negative neural networks u_θ so that $\int \widetilde{u}_\theta = 1$, the collection of \widetilde{u}_θ 's would form a sufficient large approximating class for probability density functions. Hence, it suffices to minimize

$$(3.3) \quad \arg \min_{\theta} \left\{ \mathcal{F}(\widetilde{u}_\theta) + \frac{\mathbb{W}_2^2(\widetilde{u}_\theta, u_k)}{2\tau} \right\},$$

for a given u_k to obtain the minimizer $\widetilde{u}_{\theta^*(k+1)}$, which is an approximation of the minimizer of (3.1). As in the case $X = L^2(\Omega)$, we take the optimized $\widetilde{u}_{\theta^*(k+1)}$ in place of u_k and repeat this process iteratively to derive the corresponding time-discretized gradient flow.

However, unlike the case $X = L^2(\Omega)$, there is no direct easy way to evaluate the squared metric, i.e. $\mathbb{W}_2^2(u, \rho)$, when minimizing the objective (3.3). There are many algorithms to approximate the L^2 -Wasserstein distance, but we take an idea proposed in [20] for the reasons described in Section 2.3. In other words, we approximate it by solving the optimization problem (2.12) at first and then by evaluating (2.13) using the optimal ψ_{θ^*} and ψ_{w^*} . All the integrations in formulae (2.13) and (2.12) are again evaluated by Monte Carlo as described in Section 3.1. Moreover, the non-negativity assumption on neural networks can be easily satisfied by choosing non-negative activation functions such as Softplus [14], ReLU [36], ELU [8], etc.

4. Experiments. In this section, we show through various kinds of examples, that one can accurately approximate the solutions of PDEs which have gradient flow structures via neural networks. We divide this section into two subsections, each of which is devoted to gradient flows for the case L^2 and the case \mathbb{W}_2 respectively. For the L^2 gradient flow case, we demonstrate the scalability of the proposed method to the high-dimensional problems through the heat equation. Throughout this section, we apply the domain truncation technique for the unbounded domains (in our cases \mathbb{R}^n) as applied in the literature (See, for example, [16, 7]). We compute the L^2 error of a neural network solution u_{NN} by $\|u - u_{NN}\|_{L^2}$ and the relative L^2 error by $\frac{\|u - u_{NN}\|_{L^2}}{\|u\|_{L^2}}$ where u denotes either an analytic solution or a numerical solution.

Motivating Example. We first consider a simple motivating example with the L^2 energy functional $\frac{\kappa}{2} \int_{\Omega} u^2 dx$. The corresponding minimization problem reads as :

$$(4.1) \quad \arg \min_{\theta} \left\{ \frac{\kappa}{2} \int_{\Omega} u_{\theta}^2 dx + \frac{d_{L^2(\Omega)}^2(u_{\theta}, u_k)}{2\tau} \right\},$$

where u_{θ} is a neural network solution and θ denotes the set of parameters. We set an initial condition $u(0, x) = \sin(x)$, $\Omega = [-\pi, \pi]$, then the corresponding solution of the PDE is $u(t, x) = e^{-\kappa t} \sin(x)$. In Figure 4.1, we demonstrate the minimizer $u_{\theta, k+1}$ approximately satisfies the Euler-Lagrange equation of (4.1), i.e.,

$$\frac{u_{\theta, k+1} - u_{\theta, k}}{\tau} = -\nabla F(u_{k+1}),$$

during 40 timesteps with $\tau = 0.01$.

4.1. L^2 -gradient flows. In this section, we consider two examples of L^2 -gradient flows, the heat equation and the Allen-Cahn equation.

4.1.1. Heat equation: 2-dimensional, 8-dimensional. The heat equation

$$(4.2) \quad \begin{cases} \partial_t u = \kappa \Delta u & \text{in } \Omega, \\ \nabla u \cdot \hat{\mathbf{n}} = 0 & \text{on } \partial\Omega, \end{cases}$$

where \mathbf{n} denotes the unit normal vector, is the L^2 -gradient flow of the Dirichlet energy $\mathcal{F}(u) := \frac{\kappa}{2} \int_{\Omega} |\nabla u|^2 dx$.

For the special case $\Omega = [-a, a]^n$, where the domain is given by an n -dimensional cube, the ground-truth solution of (4.2) can be computed. Let the initial condition is given by $u(0, x) = \sum_{[i]} A_{[i]} \prod_k \cos(\frac{i_k \pi x_k}{a})$. $[i] = (i_1, i_2, \dots, i_n)$ denotes the multi-index and $A_{[i]}$ is a coefficient of $\prod_k \cos(\frac{i_k \pi x_k}{a})$. Assuming the convergence of the initial

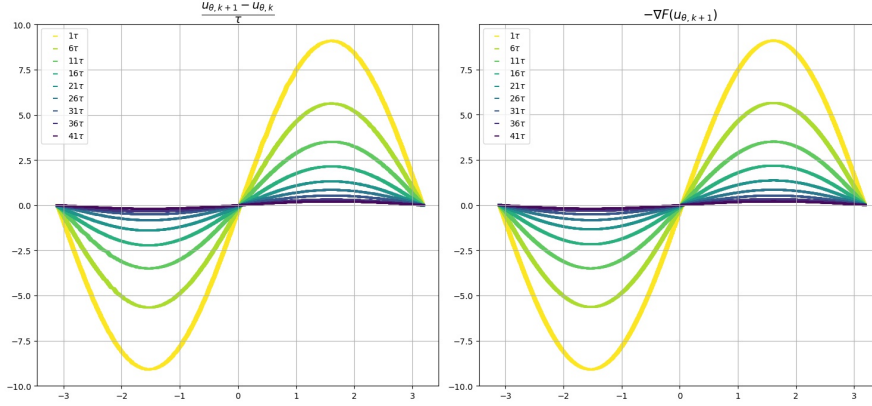


Fig. 4.1: Left: Scatter plot for the values of $\frac{u_{\theta, k+1} - u_{\theta, k}}{\tau}$ on the uniform samples. Right: Scatter plot for the values of $-\nabla F(u_{\theta, k+1})$ on the same sample points.

condition $u(0, x)$, then

$$(4.3) \quad u(t, x) = \sum_{[i]} A_{[i]} \left(\prod_k \cos\left(\frac{i_k \pi x_k}{a}\right) \right) e^{-\kappa \mu_{[i]}^2 t}, \quad \mu_{[i]}^2 = \pi^2 \sum_k \left(\frac{i_k}{a}\right)^2$$

solves (4.2) and satisfies the boundary condition.

2-dimensional case. In the experiment for 2-dimensional heat equation, we set $\kappa = 0.1$ and $a = \pi/4$. The domain Ω is given by $[-\pi/4, \pi/4]^2$. For an initial condition $u_0(x) = 4 - 0.5 \cos 4x_1 + 0.6 \cos 4x_2 + \cos 8x_1 \cos 4x_2 + \cos 8x_1 \cos 8x_2$, its ground-truth solution $u(t, x)$ is computed as in (4.3). A size of the time-step for the minimizing movement scheme is given by $\tau = 0.005$.

Model training details for 2d case. We use a 2-layer fully connected neural network with 256 hidden units for the model that approximates the solution $u(x)$. A tangent hyperbolic (tanh) activation function is applied. We choose the learning rate as 10^{-3} with an Adam [19] optimizer. While training the neural network model, we uniformly picked 10,000 samples from $\Omega = [-\pi/4, \pi/4]^2$ and computed the minimization target (3.2) by Monte-Carlo approximation.

Results - 2d case. The approximated results is illustrated in Figure 4.2. We visualized the ground-truth solution and the approximated neural network solution at the time $t = 2\tau, 20\tau, 40\tau$. Overall, the deep minimizing movement scheme achieved a good result on the 2d heat equation. Our approximated neural network solution achieved the relative L^2 error around 3.15×10^{-3} at $t = 0.2 = 40\tau$.

8-dimensional case. In the experiment for 8-dimensional heat equation, we set $\kappa = 0.25$, and $a = \pi/4$. The domain Ω is given by $[-\pi/4, \pi/4]^8$. For an initial condition $u_0(x) = 1 - 0.2 \cos 8x_2 + 2 \cos 4x_4 - \cos 4x_6 + \cos 4x_8 + 2 \cos 4x_1 \cos 4x_3 \cos 4x_8 + 2 \cos 4x_2 \cos 4x_5 \cos 4x_7$, its ground-truth solution $u(t, x)$ is computed by (4.3), the same as with the 2-dimensional case. A size of the time-step for the minimizing movement scheme is given by $\tau = 0.005$.

Model training details for 8d case. For the neural network model that approximates the solution $u(x)$, a 3-layer fully connected neural network with 256 hidden units is used. A tangent hyperbolic (Tanh) activation function is applied. We choose the learning rate as 10^{-5} with an Adam optimizer. While training the neural network

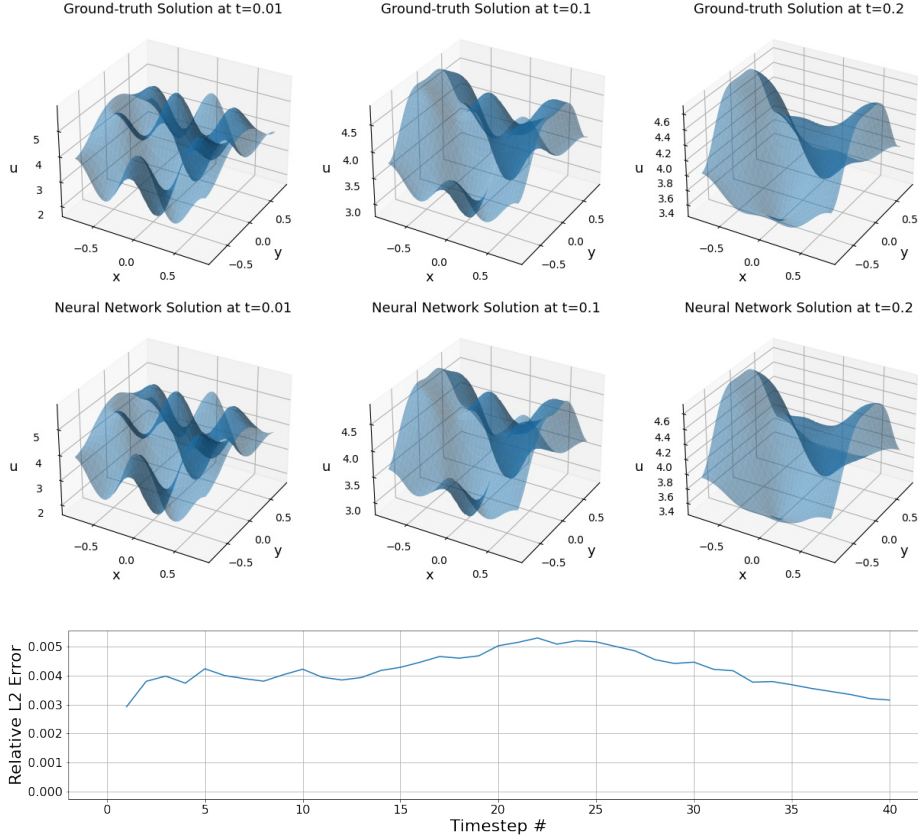


Fig. 4.2: Ground-truth solution (top row) and our neural network solution (middle row) with deep minimizing movement scheme at time $t = 0.01, 0.1, 0.2$. (At $t = 2\tau, 20\tau, 40\tau$) The relative L^2 error for each timestep is plotted in the graph at the bottom row.

model, we uniformly picked 50,000 samples from $\Omega = [-\pi/4, \pi/4]^8$ and computed the minimization target (3.2) by Monte-Carlo approximation.

Results - 8d case. For the high dimensional heat equation, we illustrated our approximated neural network solution and its relative L^2 error result in Figure 4.3, by visualizing the solution on the 4 hyperplanes $x_1x_2/x_3x_4/x_5x_6/x_7x_8$ -planes. Each solution $u_{sliced}(x_i, x_{i+1})$ was evaluated and visualized by fixing the other 6 variables to zero and varying $(x_i, x_{i+1}) \in [-\pi/4, \pi/4]^2$ for $i = 1, 3, 5, 7$. We plotted the ground-truth solution and the approximated neural network solution at the time $t = 40\tau$. Its relative L^2 error is estimated 500 times, each with 50,000 points that are uniformly sampled from the domain Ω . The deep minimizing movement scheme also achieved a good result on the 8d heat equation. Our approximated neural network solution achieved the relative L^2 error around 3.67×10^{-2} at $t = 0.2 = 40\tau$. These result clearly showed the applicability of our proposed method as a cornerstone of dealing with high dimensional PDEs.

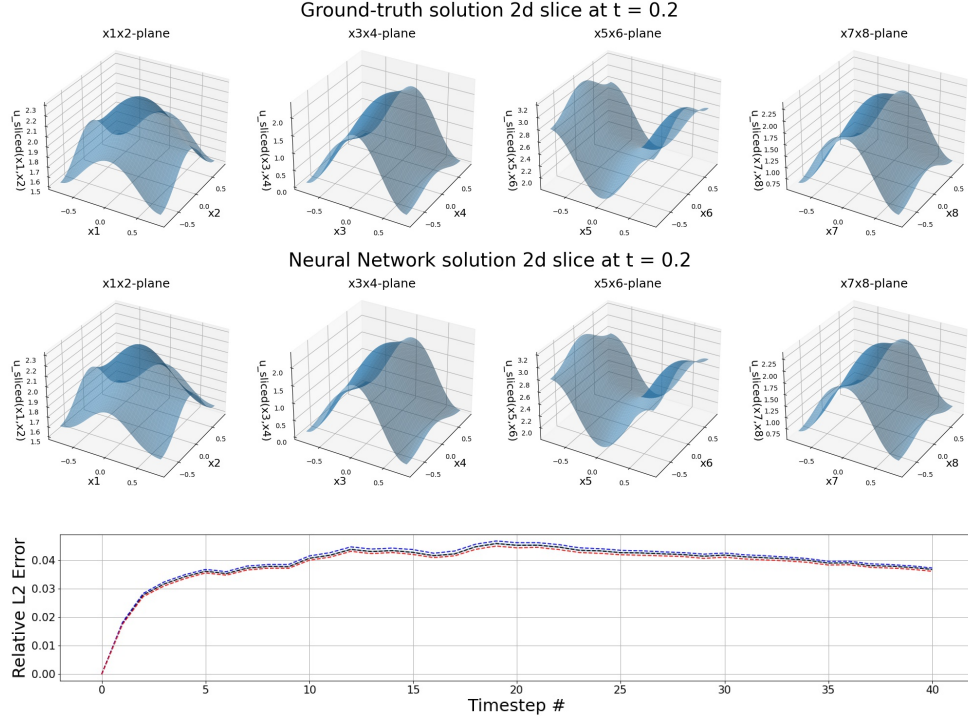


Fig. 4.3: Ground-truth solution (top row) and our neural network solution (middle row) with deep minimizing movement scheme at time $t = 0.2 = 40\tau$. The relative L^2 error for each timestep is plotted in the graph at the bottom row. In the relative L^2 error plot, we estimated the error with 500 trials, each evaluated on 50,000 points that are uniformly sampled from Ω . Blue dotted line indicates the maximum error and the red dotted line indicates the minimum error among the 500 trials for each timestep. As the plots of the maximum error and the minimum error are almost coincident, it can be deduced that the evaluated result is surely robust.

4.1.2. Allen-Cahn equation: 2-dimensional.

The Allen-Cahn equation

$$(4.4) \quad \begin{cases} \partial_t u = \Delta u - \epsilon^{-2} F'(u) & \text{in } \Omega, \\ \nabla u \cdot \hat{\mathbf{n}} = 0 & \text{on } \partial\Omega, \end{cases}$$

where \mathbf{n} denotes the unit normal vector, is the L^2 -gradient flow of the functional $I_\epsilon(u) := \frac{1}{2} \int \|\nabla u\|^2 dx + \epsilon^{-2} \int F(u) dx$ where $\epsilon > 0$ and F is a double well potential. In our experiment, we consider the case where the double well potential $F(s)$ is given by $\frac{(s^2-1)^2}{4}$. We set $\epsilon = 0.25$ and the domain $\Omega = [-2, 2] \times [-2, 2]$. The ground-truth solution of (4.4) is computed with a forward Euler scheme, where the initial condition in Fig. 4.4 is examined. A size of the time-step for the minimizing movement scheme is given by $\tau = 0.005$.

Model training details. For the neural network model that approximates the solution $u(x)$, a 2-layer fully connected neural network with 256 hidden units is used. An exponential linear unit (ELU) activation function is applied. We choose the learning rate as 10^{-3} with an Adam optimizer. As the same as 2d heat equation case, we

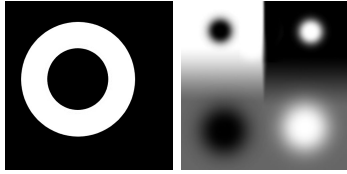


Fig. 4.4: A hard torus-shape initial condition (left) and a 4-point initial condition (right) are used for the experiment on the Allen-Cahn equation. Black color indicates -1 and white color indicates 1.

uniformly picked 10,000 samples from $\Omega = [-2, 2]^2$ and computed the minimization target.

Results. The result for the hard torus-shape initial condition and the 4-point initial condition in Fig. 4.4 is visualized in Fig. 4.5 and Fig. 4.6 respectively. The ground-truth solution is obtained with the forward Euler scheme. We visualized the ground-truth solution and the approximated neural network solution at the time $t = 2\tau, 20\tau, 40\tau$ and plotted the relative L^2 error for each timestep. The trained models for the two initial conditions at $t = 0.2 = 40\tau$ achieved its relative L^2 error 3.76×10^{-2} and 6.69×10^{-2} respectively. Although the borderline area between -1 and +1 evolves rapidly and has a steep slope, the neural network approximator and our proposed deep minimizing movement scheme achieved good results for the given two initial conditions.

4.2. \mathbb{W}_2 -gradient flows. In this section, we consider several examples of \mathbb{W}_2 -gradient flows. In the following experiments, we used the Softplus activation function for the last layer to guarantee the positivity of neural networks. Activation functions used in the remaining layers except for the last layer are specified for each experiment.

4.2.1. Heat equation: 2-dimensional. We consider

$$\begin{cases} \partial_t u = \kappa \Delta u & \text{in } [0, T] \times [-\pi, \pi]^2, \\ \nabla u \cdot \hat{n} = 0 & \text{on } [0, T] \times \partial[-\pi, \pi]^2, \\ u(0, x_1, x_2) = (1 + \frac{1}{5} \cos(x_1) + \frac{1}{5} \cos(x_2)) / (4\pi^2) \end{cases}$$

which corresponds to a \mathbb{W}_2 -gradient flow of the entropy functional $\mathcal{F}(u) := \int_{\Omega} u(x) \log u(x) dx$. ■

Model training details. In this numerical experiment, we employ a 4-layer fully connected neural network with 512 hidden units with cosine activation function. We use Adam optimizer with a learning rate 2×10^{-4} . We set $\tau = 0.005$. For each training epoch, we sample 20,000 points from $[-\pi, \pi] \times [-\pi, \pi]$ uniformly. Numerical integrations are computed by using the Monte-Carlo method.

4.2.2. Porous Medium: 1-dimensional. The porous medium equation

$$(4.5) \quad \partial_t u(t, x) = \Delta u^m, \quad \text{in } [0, T] \times \mathbb{R}^n$$

is the \mathbb{W}_2 -gradient flow of the energy $\mathcal{F}(u) : \frac{1}{m-1} \int_{\mathbb{R}^n} u^m(x) dx$.

A fundamental example of exact solution of this equation was obtained independently by Barenblatt and Pattle [6], which are densities of the form

$$(4.6) \quad u(t, x) = (t + t_0)^{-kn} \left(C - \frac{(m-1)k}{2m} \|x\|^2 t^{-2k} \right)_+^{\frac{1}{m-1}},$$

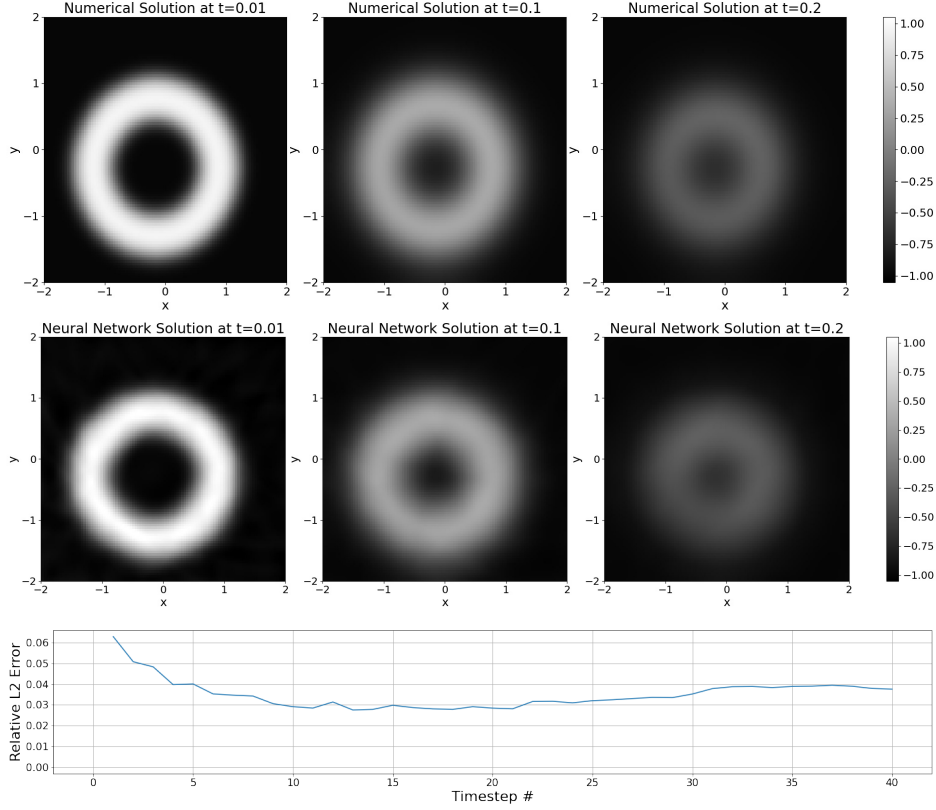


Fig. 4.5: Ground-truth numerical solution (top row) and our neural network solution (middle row) with deep minimizing movement scheme of the Allen-Cahn equation at time $t = 0.01, 0.1, 0.2$. (At $t = 2\tau, 20\tau, 40\tau$), based on the hard torus-shape initial condition. Its relative L^2 error for each timestep is plotted in the graph at the bottom row.

where $k = (n(m-1) + 2)^{-1}$ and the positive constant C is defined by the identity $\int_{\mathbb{R}^n} u(t, x) dx = 1$.

In this experiment, we set $t_0 = 10^{-1}$, $m = 2$, and $C = (\frac{3}{64})^{\frac{1}{3}}$. Moreover, we set $u(x, 0)$ in the equation (4.6) to be the initial condition.

Model training details. In this numerical experiment, we employ a 5-layer fully connected neural network with 512 hidden units with ELU activation function. We use Adam optimizer with a learning rate 2×10^{-4} . We set $\tau = 0.005$ and truncated the domain \mathbb{R} by $[-3, 3]$ so that the numerical integration of the initial condition has a negligible error. For each training epoch, we sample 3,000 points from $[-3, 3]$ uniformly. Numerical integrations in the algorithm are computed by using the Monte-Carlo method.

Results. Both the neural network solution and the ground-truth solution over time until $t = 60\tau$ are plotted in Figure 4.8 and error estimation is give in Figure 4.9. As is shown in Figure 4.8, despite the accumulation of errors over time, it fits well for a fairly long time.

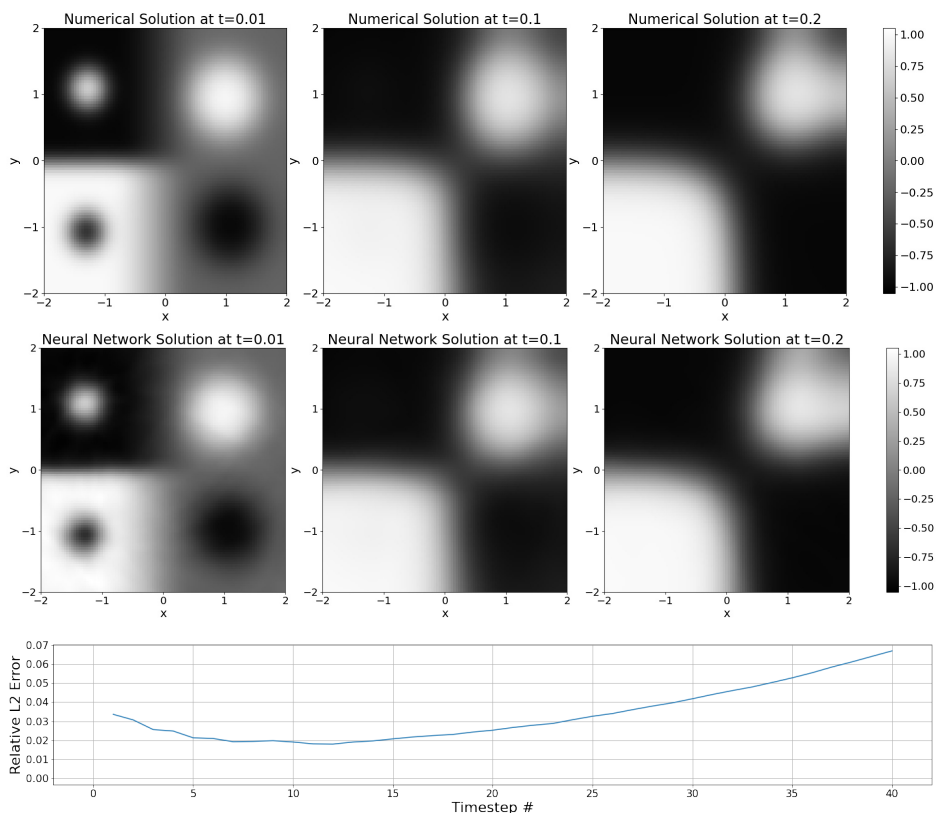


Fig. 4.6: Ground-truth numerical solution (top row) and our neural network solution (middle row) with deep minimizing movement scheme of the Allen-Cahn equation at time $t = 0.01, 0.1, 0.2$. (At $t = 2\tau, 20\tau, 40\tau$), based on the 4-point initial condition. Its relative L^2 error for each timestep is plotted in the graph at the bottom row.

4.2.3. Porous medium equation: 2-dimensional. In this experiment, we set $t_0 = 10^{-1}$, $m = 2$, and $C = \frac{1}{\sqrt{8\pi}}$. As in the 1-dimensional case, we take the $u(x, 0)$ in the equation (4.6) to be the initial condition.

Model training details. In this numerical experiment, we employ a 5-layer fully connected neural network with 512 hidden units with ELU activation function. We use Adam optimizer with a learning rate 2×10^{-4} . We set $\tau = 0.005$ and truncated the domain \mathbb{R}^2 by $[-3, 3] \times [-3, 3]$ so that the numerical integration of the initial condition has a negligible error. For each training epoch, we sample 10,000 points from $[-3, 3] \times [-3, 3]$ uniformly. Numerical integrations in the algorithm are computed by using the Monte-Carlo method.

Results. We summarize the results in Figure 4.10 and Figure 4.11. In Figure 4.10, the neural network solution and the ground-truth solution are both plotted for timesteps $t = \tau$ and $t = 60\tau$. As in the 1-dimensional case, neural network solution fits well for a fairly long time. It is worth noticing that since we sampled more points in this experiment than in the 1-dimensional experiment, the errors are smaller.

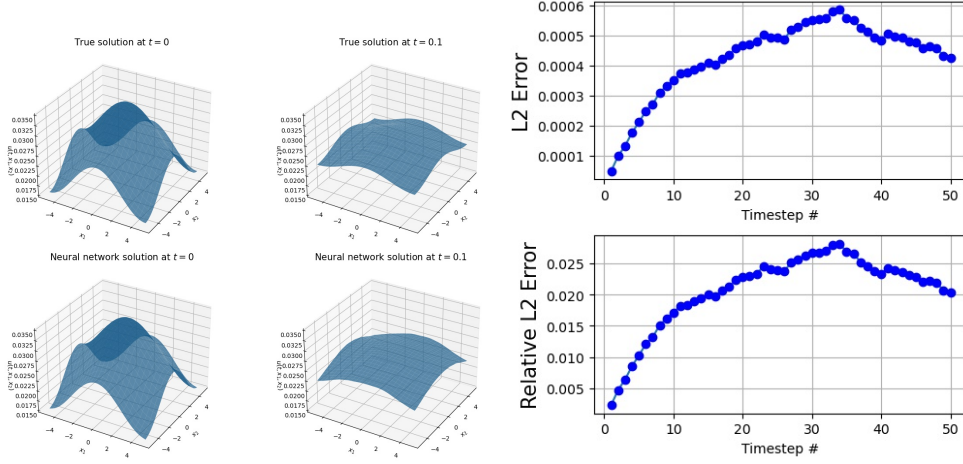


Fig. 4.7: Left: Analytic solutions and approximated solutions of (4.5) at $t = \tau, 51\tau$. Right: L^2 error and relative L^2 error of an approximated solution.

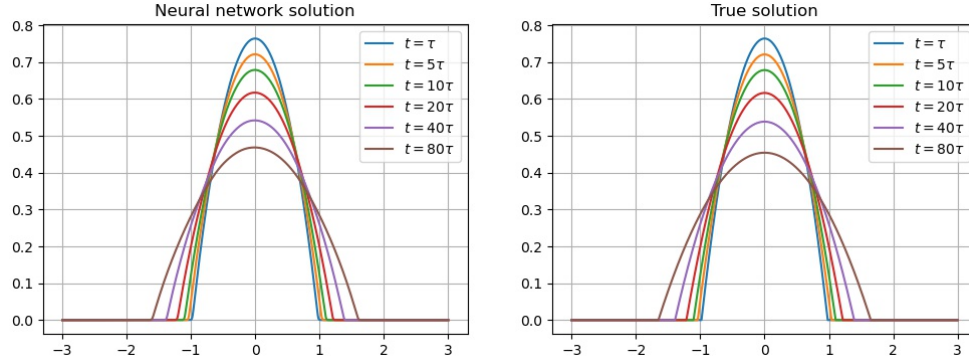


Fig. 4.8: Neural network solution and the ground-truth solution for the 1-dimensional porous medium equation over timesteps $t = \tau, \dots, 60\tau$.

4.2.4. Fokker-Planck equation: 2-dimensional. The Fokker-Planck equation

$$(4.7) \quad \partial_t u(t, x) = \nabla \cdot (u \nabla V) + \Delta u, \quad \text{in } [0, T] \times \mathbb{R}^n$$

is the \mathbb{W}_2 -gradient flow of the energy $\mathcal{F}(u) := \int_{\mathbb{R}^2} V(x)u(x) + u(x) \log u(x) dx$. In this numerical example, we set the initial condition to be the standard Gaussian distribution and set $V(x) = \frac{1}{2}(x - \mu)^T \Sigma^{-1}(x - \mu)$, with $\mu = [\frac{1}{3}, \frac{1}{3}]$, and $\Sigma = \begin{bmatrix} \frac{5}{8} & -\frac{3}{8} \\ -\frac{3}{8} & \frac{5}{8} \end{bmatrix}$.

Then, an analytic solution of (4.7) reads

$$(4.8) \quad u(t, x) = \mathcal{N}(\mu(t), \Sigma(t)) := \frac{1}{2\pi \sqrt{|\Sigma(t)|}} \exp -\frac{1}{2}(x - \mu(t))^T \Sigma(t)^{-1}(x - \mu(t)),$$

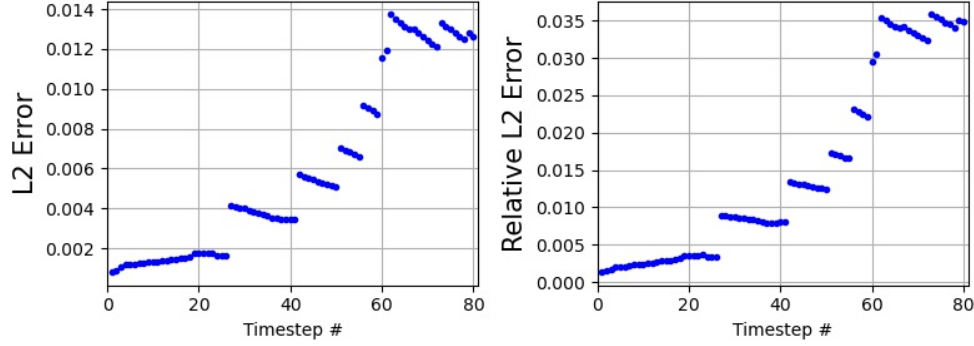


Fig. 4.9: Error estimation of the neural network solution for the porous medium equation.

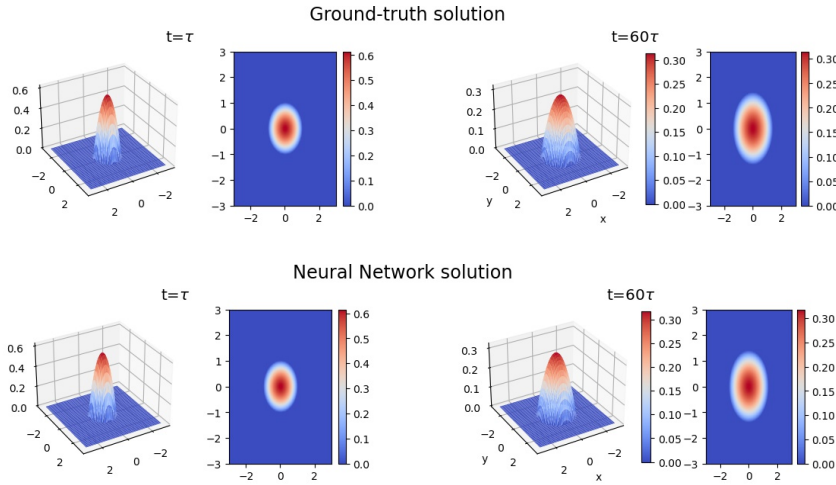


Fig. 4.10: Neural network solution and the ground-truth solution for the 2-dimensional porous medium equation for timesteps $t = \tau$ and $t = 60\tau$.

where $\mu(t) = (1 - e^{-4t})\mu$, $\Sigma(t) = \begin{bmatrix} \frac{5}{8} + \frac{3}{8} \times e^{-8t} & -\frac{3}{8} + \frac{3}{8} \times e^{-8t} \\ -\frac{3}{8} + \frac{3}{8} \times e^{-8t} & \frac{5}{8} + \frac{3}{8} \times e^{-8t} \end{bmatrix}$.

Model training details. In this numerical experiment, we employ a 4-layer fully connected neural network with 512 hidden units with ReLU activation function. We use Adam optimizer with a learning rate 2×10^{-4} . We set $\tau = 0.005$ and truncated the domain \mathbb{R}^2 by $[-5, 5] \times [-5, 5]$ so that the numerical integration of the initial condition has a negligible error. For each training epoch, we sample 10,000 points from $[-5, 5] \times [-5, 5]$ uniformly. Numerical integrations in the algorithm are computed by using the Monte-Carlo method.

Results. We summarize the results in Figure 4.12. The left panel of Figure 4.12 shows both an analytic solution (4.8) and a neural network solution at $t = \tau$, and $t = 21\tau$. The right panel of the figure shows trajectories of mean vector of an analytic

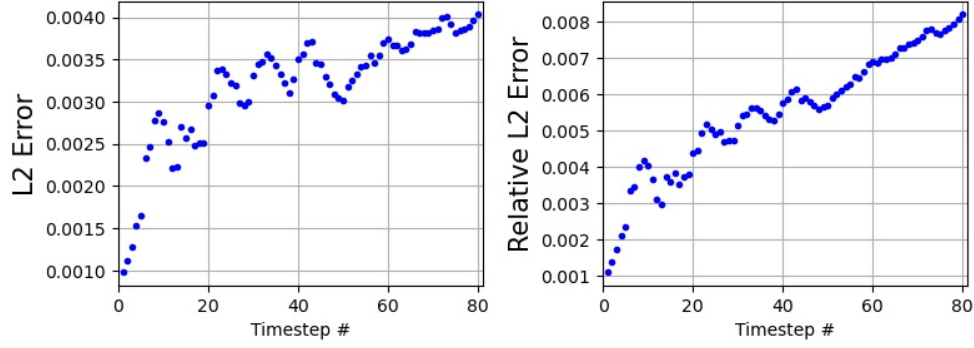


Fig. 4.11: Error estimation of the neural network solution for the 2-dimensional porous medium equation.

solution and a neural network solution. We achieved a relative error less than 0.01 (averaged in time) in the truncated domain, where u_{NN} denotes a neural network solution.

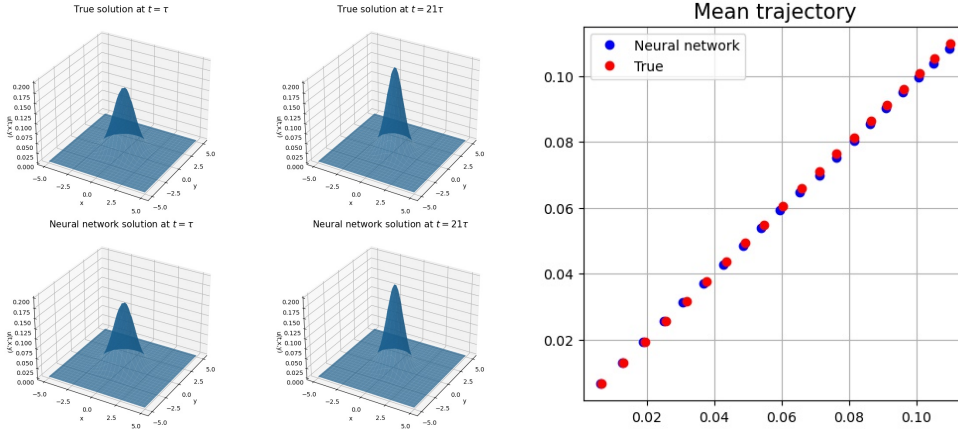


Fig. 4.12: Left: Analytic solutions and approximated solutions of (4.7) at $t = \tau, \dots, 21\tau$. Right: Mean trajectories of an analytic solution and an approximated solution.

4.2.5. Fokker-Planck equation: 4-dimensional. In this experiment, we set the initial condition to be the standard Gaussian distribution and $V(x) = \frac{1}{2}(x - \mu)^T \Sigma^{-1}(x - \mu)$ where $\mu = [\frac{1}{3}, \frac{1}{3}, 0, 0]$ and $\Sigma = \begin{bmatrix} \frac{5}{8} & -\frac{3}{8} \\ -\frac{3}{8} & \frac{5}{8} \end{bmatrix} \oplus \begin{bmatrix} 1 & 0 \\ 0 & 1 \end{bmatrix}$. In this case, the analytic solution of (4.7) is given by (4.8) where $\mu(t) = [\frac{1}{3}(1 - e^{-4t}), \frac{1}{3}(1 - e^{-4t}), 0, 0]$ and $\Sigma(t) = \begin{bmatrix} \frac{5}{8} + \frac{3}{8} \times e^{-8t} & -\frac{3}{8} + \frac{3}{8} \times e^{-8t} \\ -\frac{3}{8} + \frac{3}{8} \times e^{-8t} & \frac{5}{8} + \frac{3}{8} \times e^{-8t} \end{bmatrix} \oplus \begin{bmatrix} 1 & 0 \\ 0 & 1 \end{bmatrix}$.

Model training details. In this numerical experiment, we employ 5-layer fully connected neural network with 256 hidden units with ELU activation function. We use Adam optimizer with a learning rate 2×10^{-4} . We set $\tau = 0.005$ and truncated the domain \mathbb{R}^4 by $[-3.5, 3.5]^4$, and in this case the error of the numerical integration of the initial condition on this domain and the whole domain is less than 2%. For each training epoch, we sampled 160,000 points from $[-3.5, 3.5]^4$ uniformly. Numerical integrations in the algorithm are computed by using the Monte-Carlo method.

Results. The mean trajectories of the neural network solution and the ground-truth solution along timesteps $t = \tau, \dots, 60\tau$ are given in Figure 4.13. The first and second coordinates of the mean trajectories of both neural network solution and the ground-truth solution are in the relation $y = x$ as illustrated in the left top of Figure 4.13. The right panel of Figure 4.13 is the mean trajectories of both neural network solution and the ground-truth solution over $t = 0, \dots, 20\tau$, and it can be checked that they are overlapping.

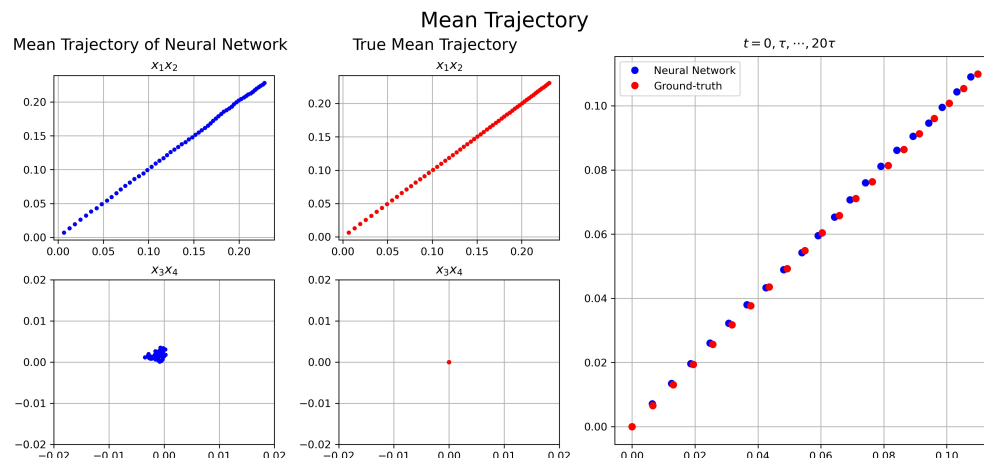


Fig. 4.13: Mean trajectories of our optimized neural network and the ground-truth solution. The trajectories taken from τ to 60τ are plotted with respect to the first and the second coordinates on the top left, and with respect to the third and fourth coordinates on the bottom left. On the right, trajectories of neural network and the ground-truth solution taken for $t = 0$ to 20τ are plotted in the same plot together for detailed comparison.

The heat maps of cross-sectional u_{sliced} 's are given in Figure 4.14. The ground-truth solution of $u_{sliced}(x_3, x_4)$ converges to a Gaussian distribution with the variance $\begin{bmatrix} \frac{5}{8} & -\frac{3}{8} \\ -\frac{3}{8} & \frac{5}{8} \end{bmatrix}$ while the ground-truth solution of $u_{sliced}(x_1, x_2)$ remains unchanged. As time goes by, the shape of the variance of the neural network solution of $u_{sliced}(x_3, x_4)$ follows $\begin{bmatrix} \frac{5}{8} & -\frac{3}{8} \\ -\frac{3}{8} & \frac{5}{8} \end{bmatrix}$. Meanwhile, even with the passage of time, the neural network solution of $u_{sliced}(x_3, x_4)$ remains the same as the standard Gaussian distribution.

Error estimation is given in Figure 4.15. The right panel of Figure 4.15 is the plot of the mean of the relative L^2 error over time, i.e. $\frac{1}{K} \sum_{k=1}^K [\text{relative } L^2 \text{ error at } t = k\tau]$.

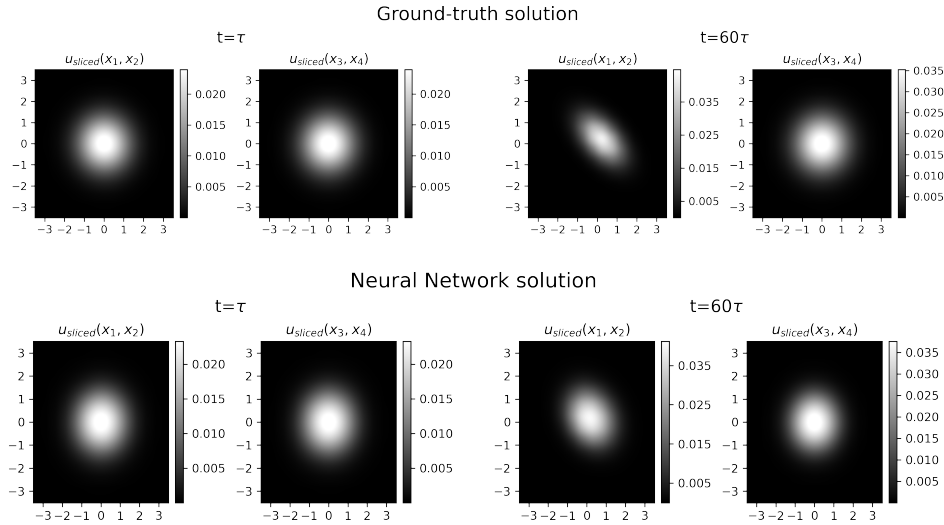


Fig. 4.14: Heat maps of cross-sectional u_{sliced} for the neural network solution and the ground-truth solution at the origin for timesteps $t = \tau$ and $t = 60\tau$ respectively. Our neural network solution for $u_{sliced}(x_1, x_2)$ becomes anisotropic, leaving $u(x_3, x_4)$ isotropic, as time passes. Since the ground-truth solution has this property, this pattern is a desiderata for approximated solutions.

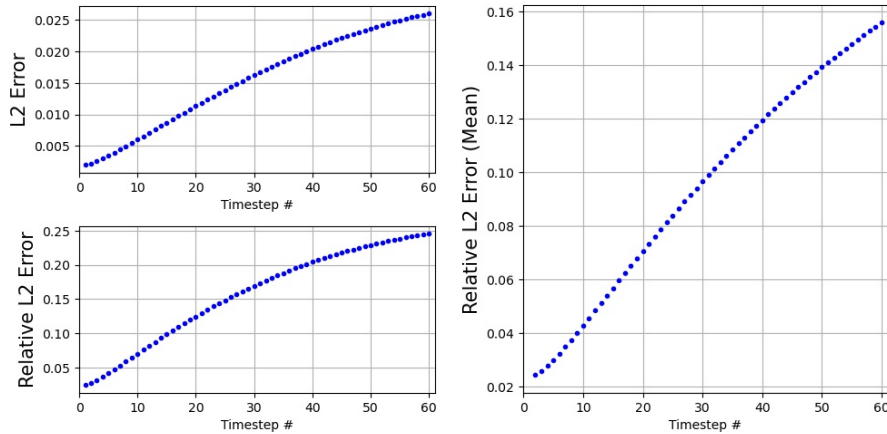


Fig. 4.15: Errors of the neural network solution for 4-dimensional Fokker-Planck equation.

5. Discussion. In the experiments on several gradient flow equations above, the proposed mesh-free deep minimizing movement scheme achieved outstanding results for both low and high dimensions. Despite lack of mature error analysis, it has been known that neural networks are more fluent than the classical numerical methods because they are free from mesh-generation. By the series of experiments in this work,

we verified that neural networks perform great for both low and high dimensions, and this indicates the possibility of applying our method to solve various PDEs related to gradient flows.

As pointed out in [4], mesh generation often fails to scale when the domain has a complex geometry. Our approach for both L^2 and \mathbb{W}_2 cases, which is completely free of mesh generation, is therefore directly applicable for the gradient-flow type equation in a domain with complex geometry. Our method also takes advantage in that it can be directly applied not only to L^2 and \mathbb{W}_2 spaces, but also to any general space. Therefore, if some classes of PDEs are realized as gradient flows in some spaces other than L^2 and \mathbb{W}_2 in future, our method can be a breakthrough for numerically solving those equations.

Acknowledgement. This work was supported by the National Research Foundation of Korea (NRF) grant funded by the Korea government (MSIT) (No. NRF-2017R1E1A1A03070105 and NRF-2019R1A5A1028324), Institute for Information & Communications Technology Promotion (IITP) grant funded by the Korea government (MSIT) (No. 2019-0-01906, Artificial Intelligence Graduate School Program (POSTECH)), and the Information Technology Research Center (ITRC) support program (No. IITP-2018-0-01441).

REFERENCES

- [1] D. ALVAREZ-MELIS, Y. SCHIFF, AND Y. MROUEH, *Optimizing functionals on the space of probabilities with input convex neural networks*, arXiv preprint arXiv:2106.00774, (2021).
- [2] L. AMBROSIO AND N. GIGLI, *A user's guide to optimal transport*, in CIME summer school, Italy, 2009, <https://hal.archives-ouvertes.fr/hal-00769391>.
- [3] B. AMOS, L. XU, AND J. Z. KOLTER, *Input convex neural networks*, in International Conference on Machine Learning, PMLR, 2017, pp. 146–155.
- [4] J. BERG AND K. NYSTRÖM, *A unified deep artificial neural network approach to partial differential equations in complex geometries*, Neurocomputing, 317 (2018), pp. 28–41.
- [5] A. BRAIDES, *Local minimization, variational evolution and Γ -convergence*, vol. 2094, Springer, 2014.
- [6] J. A. CARRILLO AND G. TOSCANI, *Asymptotic l^1 -decay of solutions of the porous medium equation to self-similarity*, Indiana University Mathematics Journal, (2000), pp. 113–142.
- [7] S. W. CHO, H. J. HWANG, AND H. SON, *Traveling wave solutions of partial differential equations via neural networks*, Journal of Scientific Computing, 89 (2021).
- [8] D.-A. CLEVERT, T. UNTERTHINER, AND S. HOCHREITER, *Fast and accurate deep network learning by exponential linear units (elus)*, arXiv preprint arXiv:1511.07289, (2015).
- [9] L. COURTE AND M. ZEINHOFER, *Robin pre-training for the deep ritz method*, arXiv preprint arXiv:2106.06219, (2021).
- [10] G. CYBENKO, *Approximation by superpositions of a sigmoidal function*, Mathematics of control, signals and systems, 2 (1989), pp. 303–314.
- [11] E. DE GIORGI, *Movimenti minimizzanti*, in Aspetti e problemi della Matematica oggi, Proc. of Conference held in Lecce, 1992.
- [12] E. DE GIORGI, A. MARINO, AND M. TOSQUES, *Problems of evolution in metric spaces and maximal decreasing curve*, Atti Accad. Naz. Lincei Rend. Cl. Sci. Fis. Mat. Natur.(8), 68 (1980), pp. 180–187.
- [13] M. DISSANAYAKE AND N. PHAN-THIEN, *Neural-network-based approximations for solving partial differential equations*, communications in Numerical Methods in Engineering, 10 (1994), pp. 195–201.
- [14] C. DUGAS, Y. BENGIO, F. BÉLISLE, C. NADEAU, AND R. GARCIA, *Incorporating second-order functional knowledge for better option pricing*, Advances in neural information processing systems, (2001), pp. 472–478.
- [15] K. HORNIK, *Approximation capabilities of multilayer feedforward networks*, Neural networks, 4 (1991), pp. 251–257.
- [16] H. J. HWANG, J. W. JANG, H. JO, AND J. Y. LEE, *Trend to equilibrium for the kinetic fokker-planck equation via the neural network approach*, Journal of Computational Physics,

- (2020), p. 109665.
- [17] H. JO, H. SON, H. J. HWANG, AND E. H. KIM, *Deep neural network approach to forward-inverse problems*, *Networks & Heterogeneous Media*, 15 (2020), pp. 247–259.
 - [18] R. JORDAN, D. KINDERLEHRER, AND F. OTTO, *The variational formulation of the fokker–planck equation*, *SIAM journal on mathematical analysis*, 29 (1998), pp. 1–17.
 - [19] D. P. KINGMA AND J. BA, *Adam: A method for stochastic optimization*, arXiv preprint arXiv:1412.6980, (2014).
 - [20] A. KOROTIN, V. EGAZARIAN, A. ASADULAEV, A. SAFIN, AND E. BURNAEV, *Wasserstein-2 generative networks*, arXiv preprint arXiv:1909.13082, (2019).
 - [21] I. E. LAGARIS, A. LIKAS, AND D. I. FOTIADIS, *Artificial neural networks for solving ordinary and partial differential equations*, *IEEE transactions on neural networks*, 9 (1998), pp. 987–1000.
 - [22] J. Y. LEE, J. W. JANG, AND H. J. HWANG, *The model reduction of the vlasov-poisson-fokker-planck system to the poisson-nernst-planck system via the deep neural network approach*, arXiv preprint arXiv:2009.13280, (2020).
 - [23] M. LESHNO, V. Y. LIN, A. PINKUS, AND S. SCHOCKEN, *Multilayer feedforward networks with a nonpolynomial activation function can approximate any function*, *Neural networks*, 6 (1993), pp. 861–867.
 - [24] X. LI, *Simultaneous approximations of multivariate functions and their derivatives by neural networks with one hidden layer*, *Neurocomputing*, 12 (1996), pp. 327–343.
 - [25] Y. LIAO AND P. MING, *Deep nitsche method: Deep ritz method with essential boundary conditions*, arXiv preprint arXiv:1912.01309, (2019).
 - [26] S. LIU, W. LI, H. ZHA, AND H. ZHOU, *Neural parametric fokker-planck equations*, arXiv preprint arXiv:2002.11309, (2020).
 - [27] L. LU, X. MENG, Z. MAO, AND G. E. KARNIADAKIS, *Deepxde: A deep learning library for solving differential equations*, *SIAM Review*, 63 (2021), pp. 208–228.
 - [28] A. MAKKUKA, A. TAGHVAEI, S. OH, AND J. LEE, *Optimal transport mapping via input convex neural networks*, in *International Conference on Machine Learning*, PMLR, 2020, pp. 6672–6681.
 - [29] R. J. MCCANN, *Existence and uniqueness of monotone measure-preserving maps*, *Duke Mathematical Journal*, 80 (1995), pp. 309–323.
 - [30] L. MCCLENNY AND U. BRAGA-NETO, *Self-adaptive physics-informed neural networks using a soft attention mechanism*, arXiv preprint arXiv:2009.04544, (2020).
 - [31] M. MIZUNO AND Y. TONEGAWA, *Convergence of the allen–cahn equation with neumann boundary conditions*, *SIAM Journal on Mathematical Analysis*, 47 (2015), pp. 1906–1932.
 - [32] P. MOKROV, A. KOROTIN, L. LI, A. GENEVAY, J. SOLOMON, AND E. BURNAEV, *Large-scale wasserstein gradient flows*, arXiv preprint arXiv:2106.00736, (2021).
 - [33] G. MONGE, *Mémoire sur la théorie des déblais et des remblais*, *Histoire de l’Académie Royale des Sciences de Paris*, (1781).
 - [34] J. MÜLLER AND M. ZEINHOFER, *Deep ritz revisited*, arXiv preprint arXiv:1912.03937, (2019).
 - [35] J. MÜLLER AND M. ZEINHOFER, *Notes on exact boundary values in residual minimisation*, arXiv preprint arXiv:2105.02550, (2021).
 - [36] V. NAIR AND G. E. HINTON, *Rectified linear units improve restricted boltzmann machines*, in *Icml*, 2010.
 - [37] F. OTTO, *The geometry of dissipative evolution equations: the porous medium equation*, *Communications in Partial Differential Equations*, 26 (2001).
 - [38] A. PRATELLI, *On the equality between monge’s infimum and kantorovich’s minimum in optimal mass transportation*, in *Annales de l’Institut Henri Poincaré (B) Probability and Statistics*, vol. 43, Elsevier, 2007, pp. 1–13.
 - [39] M. RAISSI, P. PERDIKARIS, AND G. E. KARNIADAKIS, *Physics-informed neural networks: A deep learning framework for solving forward and inverse problems involving nonlinear partial differential equations*, *Journal of Computational Physics*, 378 (2019), pp. 686–707.
 - [40] F. SANTAMBROGIO, *Optimal transport for applied mathematicians*, Birkäuser, NY, 55 (2015), p. 94.
 - [41] J. SIRIGNANO AND K. SPILIOPOULOS, *Dgm: A deep learning algorithm for solving partial differential equations*, *Journal of Computational Physics*, 375 (2018), pp. 1339–1364.
 - [42] H. SON, J. W. JANG, W. J. HAN, AND H. J. HWANG, *Sobolev training for the neural network solutions of pdes*, arXiv preprint arXiv:2101.08932, (2021).
 - [43] A. TAGHVAEI AND A. JALALI, *2-wasserstein approximation via restricted convex potentials with application to improved training for gans*, arXiv preprint arXiv:1902.07197, (2019).
 - [44] R. VAN DER MEER, C. OOSTERLEE, AND A. BOROVYKH, *Optimally weighted loss functions for solving pdes with neural networks*, arXiv preprint arXiv:2002.06269, (2020).

- [45] C. VILLANI, *Topics in optimal transportation*, vol. 58, American Mathematical Soc., 2003.
- [46] S. WANG, X. YU, AND P. PERDIKARIS, *When and why pinns fail to train: A neural tangent kernel perspective*, arXiv preprint arXiv:2007.14527, (2020).
- [47] E. WEINAN AND B. YU, *The deep ritz method: a deep learning-based numerical algorithm for solving variational problems*, Communications in Mathematics and Statistics, 6 (2018), pp. 1–12.